Luminescent Gold Nanoclusters Interacting with Synthetic and Biological Vesicles

Journal:	*The Journal of Physical Chemistry Letters*
Manuscript ID	jz-2022-01071t.R1
Manuscript Type:	Letter
Date Submitted by the Author:	n/a

Complete List of Authors:	Chiechio, Regina; Dipartimento di Fisica e Astronomia "Ettore Majorana", Università Di Catania Ducarre, Solene; Université de Rennes 1, Institut des Sciences Chimiques de Rennes CNRS UMR 6226 Moulin, Gregory; Rennes 1 University, Service de Biologie de la Reproduction-CECOS, Dupont, Aurelien; Universite de Rennes 1, CNRS, Inserm, BIOSIT Marets, Célia; Université de Rennes 1 Even-Hernandez, Pascale; Universite de Rennes 1, Artzner, Franck; Centre National de la Recherche Scientifique, Physics CNRS UMR 6251 Musumeci, Paolo; University of Catania, Physics Franzo, Giorgia; Istituto per la Microelettronica e Microsistemi Consiglio Nazionale delle Ricerche, MATIS, Dipartimento di Fisica e Astronomia Università di Catania Ravel, Celia; Universite de Rennes 1, Institut de Recherche en Santé, Environnement et Travail (Irset) Lofaro, Maria; University of Catania , Physics and Astronomy Department "E. Majorana" Marchi, Valerie; Universite de Rennes 1, Institut des Sciences Chimiques de Rennes

Luminescent Gold Nanoclusters Interacting With Synthetic and Biological Vesicles

Regina M. Chiechio [a,b,f], Solène Ducarre [a], Grégory Moulin [a,d], Aurélien Dupont [g], Célia Marets [a], Pascale Even-Hernandez [a], Franck Artzner [c], Paolo Musumeci [b], Giorgia Franzò [f], Célia Ravel[d,e], Maria José Lo Faro [b,f], Valérie Marchi [a]*

a Université Rennes 1, CNRS UMR 6226, Institut des Sciences Chimiques de Rennes, Avenue du général Leclerc, 35042 Rennes Cedex, France

b Dipartimento di Fisica e Astronomia "Ettore Majorana", Università Di Catania, Via Santa Sofia 64, 95123, Catania, Italy

c Université Rennes 1, CNRS UMR 6251, Institut de Physique de Rennes, Avenue du général Leclerc, 35042 Rennes Cedex, France

d CHU Rennes, Service de Biologie de la Reproduction-CECOS, 35000 Rennes, France

e Univ Rennes, Inserm, EHESP, Irset (Institut de Recherche en Santé, Environnement et Travail) - UMR_S 1085, F-35000 Rennes, France

f IMM-CNR, Via S. Sofia 64, 95123 Catania, Italy

g CNRS, Inserm, BIOSIT – UMS 3480, Univ Rennes, US_S 018, F-35000 Rennes, France

AUTHOR INFORMATION

Corresponding Author

* to whom correspondence should be addressed: valerie.marchi@univ-rennes1.fr

ABSTRACT.

According to their high electron density and ultra-small size, gold nanoclusters (AuNCs) have unique luminescence and photo-electrochemical properties that make them very attractive for various biomedical fields. These applications require a clear understanding of their interaction with biological membranes. Here we demonstrate the ability of the AuNCs as markers for lipidic bilayer structures such as synthetic liposomes and biological extracellular vesicles (EVs). The AuNCs can selectively interact with liposomes or EVs through an attractive electrostatic interaction as demonstrated by zetametry and fluorescence microscopy. According to the ratio between nanoclusters and vesicles, the lipidic membranes can be fluorescently labeled without altering their thickness until charge reversion, the AuNCs being located at the level of the phosphate headgroups. In presence of an excess of AuNCs, the vesicles tend to adhere and aggregate. The

strong adsorption of AuNCs result in the formation of a lamellar phase as demonstrated by cryo-TEM and SAXS techniques.

TOC GRAPHICS

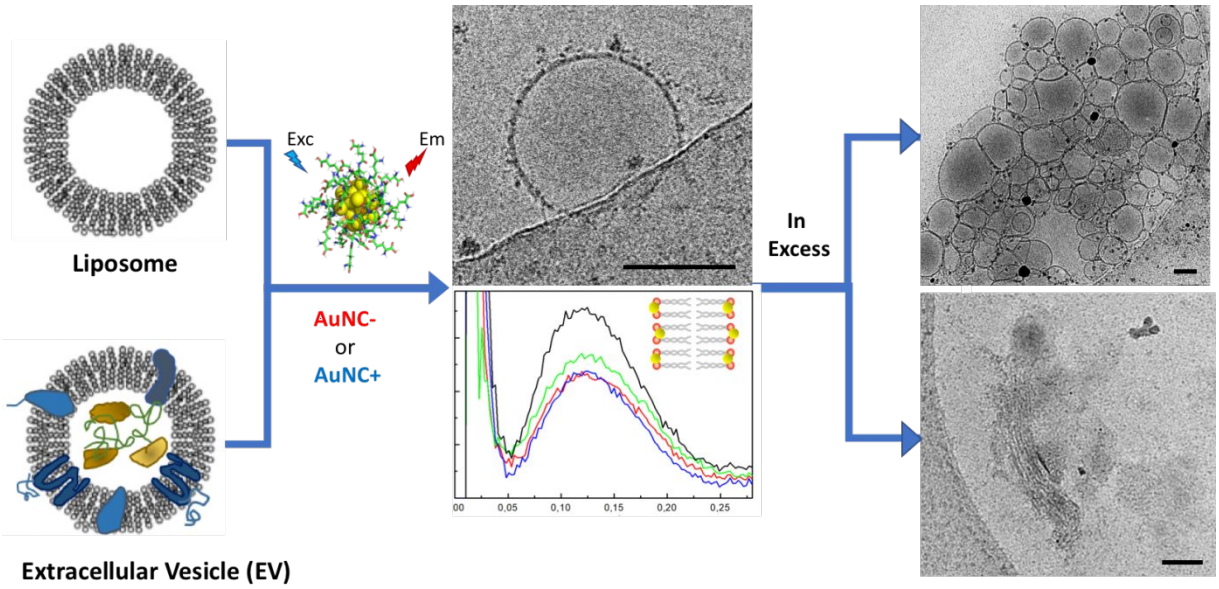

KEYWORDS gold nanoclusters, Extracellular Vesicles, liposomes, nanoparticle interacting with membrane, luminescence, biomarkers

Gold nanoclusters (AuNCs) appear as a recent class of non-toxic fluorophores. Their brightness, their ultrasmall size (< 2 nm) and large window of fluorescence lifetime (1ns - 1µs) and their good biocompatibility make them an attractive alternative as fluorescent probes for biological labeling and bioimaging.[1,2,3] Their size approaches the Fermi wavelength of electrons between metal atoms and nanoparticles. It results in molecule-like properties, including discrete energy levels and size-dependent fluorescence of the specific electronic structures. Because of its high electron density,

the presence of gold element can be detected by high resolution electron microscopy imaging. In addition, their ultra-small size facilitates their clearance when they are injected into the body. In particular gold nanoclusters are able to be filtered from the kidney and urinary excretion rapidly subsequently reducing their accumulation in the liver or spleen.[4,5,6] Multifunctional nanoconjugates based on AuNCs have been applied in tumor imaging[7,8].

Understanding their interactions with biological membranes is of direct relevance to evaluate nanotoxicity, to conceive the design of nanoparticle vectors and to control biological membrane targeting. The AuNCs could serve potentially as membrane biomarkers[9,10] or building-block for nanovector design.[11,12,] Gold nanoclusters have been used to track and visualize breast cell derived EVs into their parent cells from early endocytosis and lysosomal degradation[13]. They were also found to self-assemble with EVs to form larger defined supraparticles.[13] Due to the visco-elastic properties of lipid membranes, interacting nanoparticles can induce membrane deformation if the attractive interaction is strong enough to balance with the energetic bending cost.[12] For example, electrostatically interacting quasi-spherical quantum dots[14] or nanorods[15] can deform model membranes into egg-box-like structured lamellae or corrugated sheets. Recently, the size dependence of electrostatic interactions between gold nanoparticles (with a diameter between 5

and 40 nm) has been demonstrated.[16] This study shows that the smaller the particles are, the more they are able to induce a strong deformation of the membrane.

Here we investigate the interaction between biocompatible luminescent gold nanoclusters (AuNCs) (with a diameter lower than 2 nm) and synthetic liposomes of different sizes (with a diameter between 20 nm and 10 μm approximatively) or biological human extracellular vesicles. EV is the generic term for particles naturally released from the cell that are delimited by a lipid bilayer without any functional nucleus. These vesicles are membrane-limited particles that are secreted by healthy and cancerous cells. EVs are heterogeneous in size and three subtypes are described depending on the location of secretion: microvesicles, myelinosomes and exosomes.[17,18] A specific human fluid particularly rich in extracellular vesicles was selected to better understand the mechanism of their interaction with AuNCs. Indeed EVs are identified in follicular fluid as a mode of communication in the ovarian follicle.[19] In addition EVs involved in cell-cell communication are considered as biomarkers for early cancer diagnosis.[20–24] Their labeling with easily detectable nanoparticles could enable the development of a powerful tool for the early diagnosis of specific diseases.

We first synthetize biocompatible luminescent positively (AuNC+) or negatively (AuNC-) charged gold nanoclusters. We choose the strong and long-range electrostatic interaction to magnify any possible interaction with the membrane. The AuNCs of various surface charges were synthetized in two steps: firstly the synthesis of glutathione stabilized AuNCs according to the literature[25] by using a higher temperature to speed up its kinetics and secondly a ligand exchange with pegylated peptides of high affinity for gold surface.[26] Typically, a solution containing the glutathione reductant (GSH) and gold (III) salts was heated at boiling point for 2 hours in order to obtain the GSH NCs suspension (Figure 1a). The analysis of the TEM images (Figure 1b) reveals the crystalline structure of the NCs and their ultra-small dimensions with a diameter of 1-2 nm. Due to quantum confinement,[27,28] the NCs do not have the collective plasmon excitation typical of nanoparticles (NPs) and have composition and size-dependent fluorescence properties. As expected, the GSH NCs exhibit a maximum of fluorescence intensity peaked at 620 nm (Figure 1c). The excitation spectrum exhibits a typical peak corresponding to the Au atoms excitation with a maximum at 410 nm (Fig. 1c). The absorption spectrum presents a strong absorption due to the scattering below 350 nm masking the absorption peak of the AuNC.

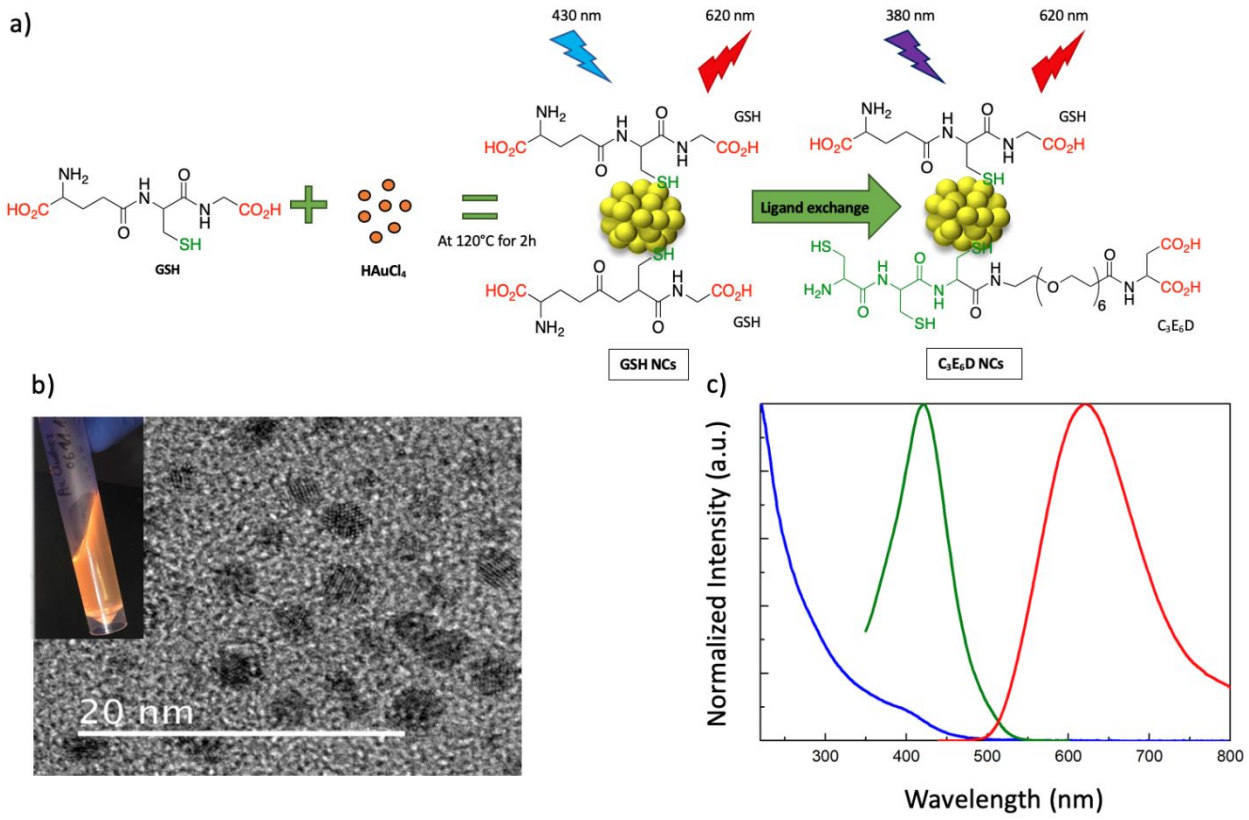

Figure 1. (a) Schematic view of the synthesis route to prepare glutathione (GSH) Gold nanoclusters followed by ligand exchange. **(b)** HR-TEM images of GSH Au NCs. Scale bar 20 nm. GSH Au NCs solution under UV lamp in the inset. **(c)** Optical properties of GSH Au NCs: (Blue) UV-Vis spectrum, (Green) Normalized Excitation spectrum (620 nm) and (Red) Normalized fluorescence emission spectrum (430 nm).

The diameter size histogram obtained by the TEM images analysis present a rather small polydispersity around 2 nm (1.2 - 2.4 nm). The fluorescence lifetime measurements exhibit a better fit using two exponential decays (Figure S1) corresponding to two lifetimes (τ_1 = 3.1 ± 0.02 µs

and $\tau_2 = 0.67 \pm 0.02\mu s$). This observation could be attributed to two different emission processes from to the surface (ligand-metal interaction) or from the AuNC core.[29] Even after lyophilization, the AuNCs are very easy to resuspend in water without any detectable aggregation or loss in luminescence (Figure S2).

To increase the AuNCs colloidal stability, three cysteine pegylated peptides negatively (C_3E_6D and C_5PEG_4) or positively charged (K_5CNH_2) (see Figure S3) were selected for their high ligand affinity according to our previous works.[30,31] In this study we also used successfully the commercial positively charged MUTAB (Mercapto-Undecyl-Trimethyl Ammonium Bromide) compound as an alternative to K_5CNH_2 compound. It is noticeable that the MUTAB single thiolate ligand with a permanent trimethyl ammonium charge regardless the pH, is only suitable for in vitro experiments because of its potential toxicity. The ligand exchange allows to obtain nanoclusters with a higher biocompatibility and stability against aggregation in aqueous buffer media due to the presence of the PEG and the terminal charges of the aspartic carboxylate or ammonium groups. The C_3E_6D NCs are also bioactivable through binding a functional targeting group (antibodies, recognition proteins, drugs) to the terminal carboxylic groups for further diagnostic and therapeutic applications. After overnight incubation in the presence of a large excess of one ligand (C_3E_6D, K_5CNH_2 or MUTAB), the GSH NCs suspension was purified by size exclusion ultracentrifugation in order to remove the free ligands and the glutathione excess to isolate the corresponding NCs. After C_3E_6D ligand exchange, the C_3E_6D AuNCs emission remains at 620 nm but the excitation varies due to the ligand exchange on the surface, going from 430 nm to 380 nm.[32] The presence of the PEG, in addition increasing the colloidal stability of AuNCs, is also able to increase its fluorescence intensity (Figure S4a, b), in agreement with previous reports in the case of thiol

PEGylated ligand,[33] by increasing the fluorescence quantum yield (3% for GSH AuNCs and 6% after C_3E_6D ligand exchange). This observation may be attributed to the rigidification of the external shell permitting to decrease the energy loss due to intramolecular vibrations and rotations.[34,35] The C_3E_6D AuNCs were kept in solution without any aggregation for one year and the fluorescence remain almost constant after 120 days (Figure S4c,d). The FT-IR spectra of the purified C_3E_6D-AuNC and GSH-AuNC have been recorded as well as those of the C_3E_6D and GSH alone (Figure S5 a and b). The two ligands exhibit two peaks assigned to amide II and amide I bonds at 1540cm^{-1} and 1650cm^{-1}. The presence of the C_3E_6D is confirmed by the two peaks assigned to the methylene vibration at 2922 cm^{-1} and 2850 cm^{-1} that are absent in the case of GSH alone. The same ligand exchange was successfully performed with the C_5PEG_4 negatively charged derivative bearing an additional undecyl chain as hydrophobic spacer between the tricystein anchor and the PEG hydrophilic part. Positively charged NCs were prepared with the positively charged K_5CNH_2 or MUTAB compounds (Figure S3). Thus, this synthesis including the ligand exchange step allows to obtain AuNCs of various surface charge which are stable against aggregation in water, biocompatible and fluorescent with a 620 nm emission wavelength fixed by the nanocluster size.

Due to their ultra-small size, these biocompatible nanostructures could label lipidic biomembranes. In this perspective, we investigate the interaction of these gold nanoclusters with model membranes and EVs from follicular human fluid and how modification of their surface properties influences this interaction. In this view, Large Unilamellar Vesicles (LUVs, about 100 nm of diameter) were synthesized by extrusion method and their size distribution measured by

DLS is presented in Figure S6. The positively charged (DOPC/DOTAP 9:1) vesicles were made to interact with the negatively (C_3E_6D AuNCs or C_5PEG_4 AuNCs) and positively charged NCs (K_5CNH_2 AuNCs or MUTAB AuNCs). The nanoclusters were prepared from the same batch of GSH NCs obtained by gold reduction with glutathione used previously. Only the ligand exchange step was adapted to vary the charge of the NCs (Figure 2a,b).

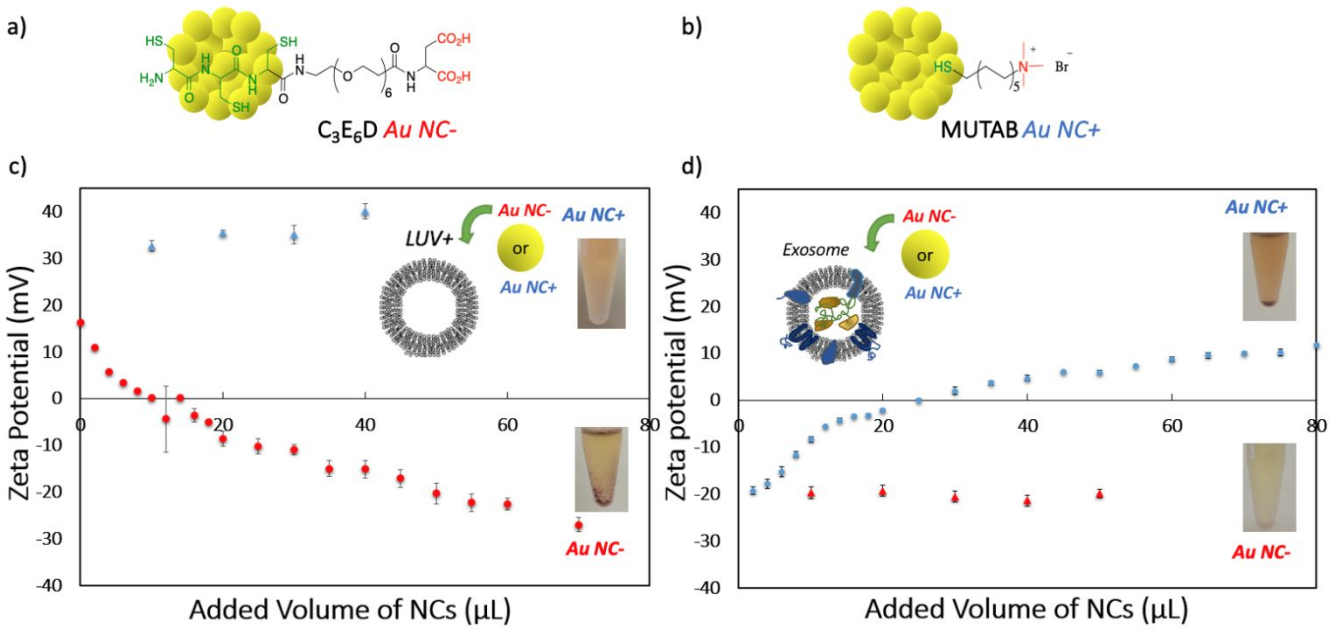

Figure 2. Schematic structure of ligand Exchanged **(a)** negatively charged C_3E_6D AuNC- (red) and **(b)** positively charged MUTAB AuNC+ (blue). **(c)** Evolution of the zeta potential during the titration of positively charged DOPC:DOTAP (9:1) Large Unilamellar Vesicles (LUVs) Liposomes (total lipid concentration 1 mM) with negatively charged C_3E_6D AuNC- (red) or positively charged MUTAB AuNC+ (blue). **(d)** Evolution of the zeta potential during the titration

of negatively charged exosomes with negatively charged C_3E_6D AuNC- (red) and positively charged MUTAB AuNC+ (blue).

The titrations of the LUVs and the EVs with oppositely charged AuNCs were performed and the surface charge evolution was followed by measuring the electrostatic Zeta potential of the vesicles. In the case of oppositely charged AuNC and LUVs, the Zeta potential decreases indicating that the negatively charged NCs neutralize the positive surface charge of the liposome until charge inversion. This behavior is attributed to the saturation of the surface vesicle due to an excess of negatively charged NCs. Finally the suspension precipitated slowly after the end of the titration. As the electrostatic interaction between vesicles and AuNC results in a charge reversion of the vesicles, the AuNC and the vesicles covered with AuNC can further interact to form condensed precipitate stabilized by electrostatic forces as observed in the case of DNA macromolecules or Quantum dots and cationic lipids.[14] As a control experiment, in presence of positively charged NCs (MUTAB AuNCs), an initial increase of the zeta potential from 15 to 40 mV is observed due to the additional contribution of the positively charged AuNCs to the mean zeta potential. When the AuNCs amount increases, there is no further variation of the Zeta potential and no final precipitation suggesting that the NCs and the vesicles keep their surface charge, the repulsive

electrostatic forces preventing colloidal instability (Figure 2c). Similar results were obtained by titration of positively charged liposomes with negatively charged C_5PEG_4 NCs or positively charged K_5CNH_2 NCs (Figure S7).

The same titrations were performed with EVs extracted from follicular liquid. As previously observed for liposomes, the negative surface charge of the exosomes was decreased by interaction with oppositely charged nanoclusters (MUTAB AuNCs) until reaching a plateau whereas no variation was observed for the surface charge in the presence of equally charged nanoclusters C_3E_6D NCs (Figure 2d). As a charge reversion was observed during the titration of both, liposomes or exosomes, a clear interaction between the lipidic membranes through electrostatic is demonstrated resulting in a precipitation after the charge reversion.

The precipitates were analyzed by two complementary techniques to in-situ investigate the structuring of nanoparticles/lipidic membranes mixtures.[15,14] The SAXS (Small Angle X-Ray Scattering) of the final precipitate obtained starting from the LUV exhibits the signature of a lamellar structure (see Figure 3a). Under the conditions of the cryo-TEM microscopy, it is noticeable that the AuNC are difficult to be detected together with the vesicles. We focus then the analysis on the vesicle membranes. The corresponding cryo-TEM images of the LUVs alone

(Figure 3 c,e) and the final precipitate (Figure 3g) reveal the presence of strongly adhered vesicles in the precipitate induced by the presence of the AuNCs. In the case of the EVs, the SAXS shows the appearance of two broad peaks corresponding to a lamellar phase (Figure 3b) which is confirmed by cryo-TEM images of EVs alone (Figure 3 d,f) and the corresponding precipitates (Figure 3h). Almost all the EVs have disrupted to form condensed lamellar phase whereas the synthetic vesicles remain only aggregated and adhered without disruption of the vesicular membrane.

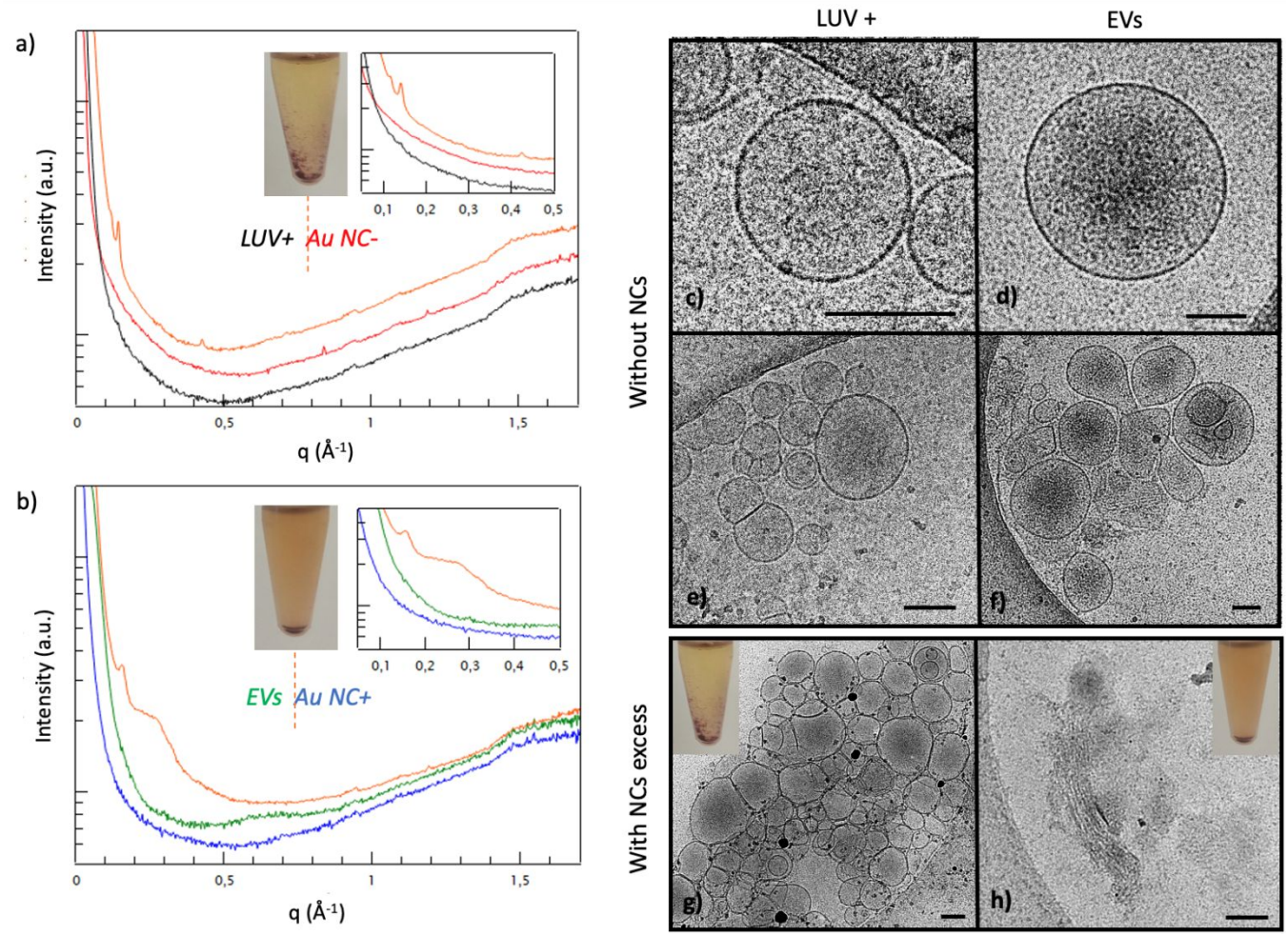

Figure 3. SAXS of the precipitate obtained at the end of the Zetametry titration study of **(a)** LUV+ and AuNC- and **(b)** EVs and AuNC+ after two weeks of incubation time: (orange) precipitate showing the appearance of two peaks, (black) LUV+, (green) EVs, (red) AuNC- and (blue) AuNC+ alone. Cryo-TEM images (scale bar 100 nm) of LUV + **(c,e,g)** and of EVs **(d,f,h)** at different magnification without AuNCs **(c,e,d,f)** and with an excess of C_3E_6D AuNC- **(g,h)** at the end of the Zetametry titration.

A complementary analysis was performed by SAXS to follow the formation of the lamellar phase. The X-ray capillaries (diameter 1.5 mm) were filled with a solution of DMPC:DMTAP (9:1) SUV+ and then the suspensions of C_3E_6D AuNC- or MUTAB AuNC+ were added in large excess on the top to create a contact surface between the two suspensions. Due to the lipid concentration required for SAXS experiments, Small Unilamellar Vesicles (SUVs) of about 50 nm diameter (Figure S6c,d) were prepared by sonication from a lipid mixture at a higher concentration (20 mg/mL) following well-known protocols.[14] The capillaries were held at room temperature for 48 hours to allow self-diffusion of AuNC and SUV+. The obtained SAXS spectra recorded at different heights in the capillary confirm the transition from a lamellar lipidic phase corresponding to the SUV+ alone with two peaks at 0.08 $Å^{-1}$ and 0.16 $Å^{-1}$ towards a hybrid phase in presence of the AuNC- with two peaks at at 0.07 $Å^{-1}$ and 0.13 $Å^{-1}$ (Figure S8a) whereas as no such transition was observed in the case of the AuNC+ (Figure S8b). In the case of neutral DMPC SUV the presence of AuNCs does not induce such behavior (Figure S8c,d). In all the cases presented, through the WAXS analysis it is noteworthly that the lipid chains remain crystalline even in presence of the NCs. The same SAXS experiments were performed with EVs from human follicular fluid. As the exosome membrane present a complex composition, the spectra do not

exhibit clear diffraction peak corresponding to the lamellar lipidic packing (Figures S9). As controls, MUTAB solutions of various concentration in presence of EVs or not do not present any diffraction peak so that the MUTAB ligand itself is not involved in the change of SAXS EVs spectrum (Figure S10). A slight intensity increase was observed in the range of 0.15 $Å^{-1}$ only in the case of the Au NC+ that is attributed to the presence of the NCs at the bilayer surface of the EVs (Figure S9b). As a conclusion, the cryo-TEM images and the SAXS measurements permit to precise that the strong electrostatic interaction between nanoclusters and vesicles results in the formation of a hybrid lamellar phase composed of the lipid membranes and the NCs.

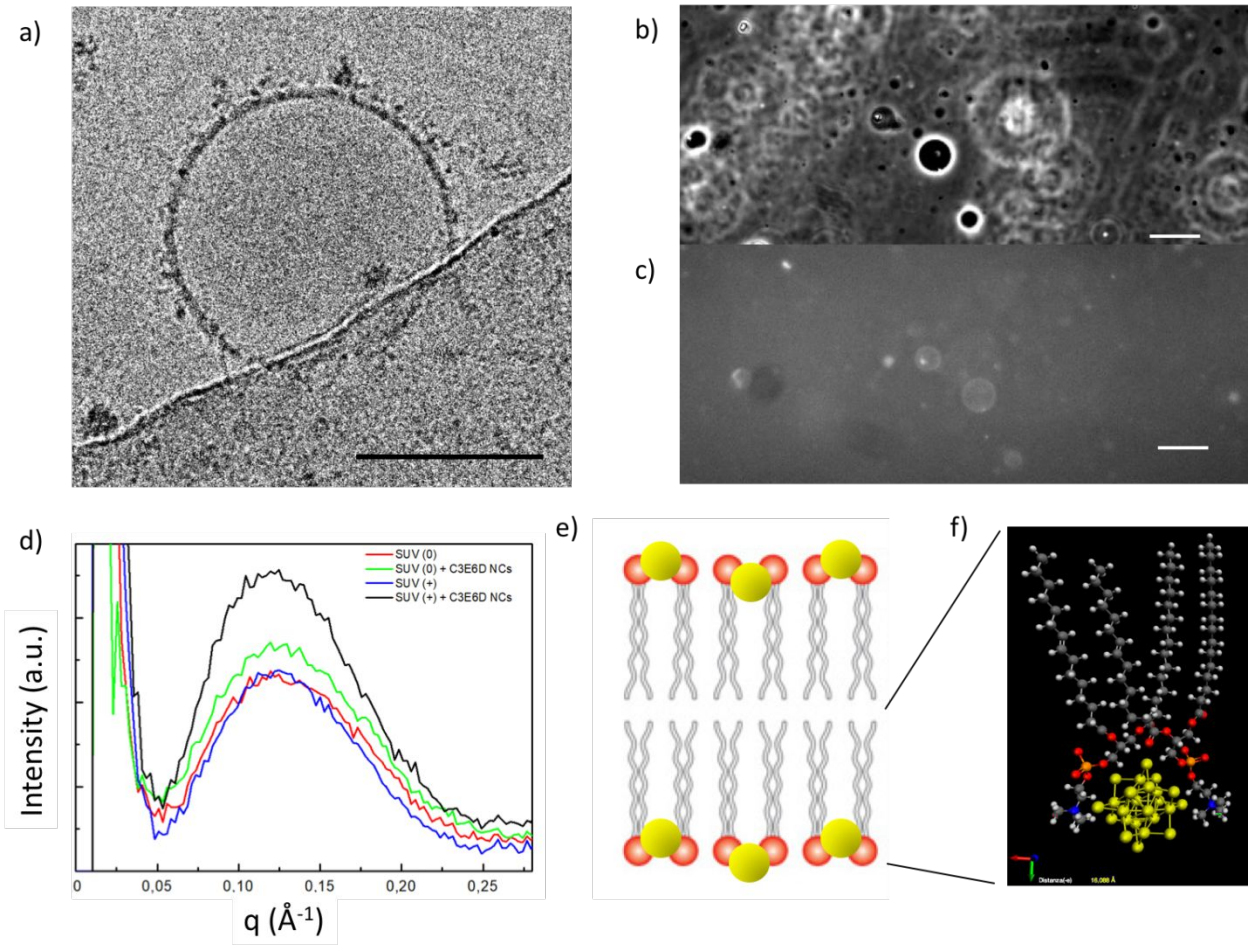

Figure 4. **(a)** Cryo-TEM images (scale bar 100 nm) of LUV+ incubated with of C_3E_6D AuNC-. Optical microscopy Images (scale bar 50 µM) of GUV+ (Giant Unilamellar Vesicles) interacting with C_3E_6D AuNC- obtained **(b)** by phase contrast and **(c)** by fluorescence. **(d)** SAXS spectra of DMPC:DMTAP (9:1) positively charged Unilamellar SUV+ alone (in blue) or in presence of C_3E_6D AuNC- (in black) and SAXS spectra of DMPC Unilamellar SUV alone (in red) or in presence of a suspension of C_3E_6D AuNC- (in green). **(e)** Schematic view and **(f)** Avogadro

simulation of AuNCs positioning between the polar heads of membrane phospholipids in the case of electrostatic attraction.

The cryo-TEM images exhibit black points of strong electron density in the vicinity of the oppositively charged membranes of LUVs that could be attributed to the presence of AuNCs (Figure 4a). To confirm this observation, the fluorescence properties of AuNCs were then exploited to visualize them at the surface of vesicles. Giant Unilamellar Vesicles (GUVs) of diameter in the micrometer range, were synthetized according to the Water-in-Oil Emulsion Transfer Methods[36] and incubated in presence of the NCs. The positively charged GUVs in excess were incubated for one hour in presence of C_3E_6D NCs (negatively charged) and then visualized under a fluorescence optical microscope which allows to see the location of the fluorescent AuNCs. The fluorescence is localized on the surface of GUVs (Figures 4b,c), indicating that the AuNCs were attracted to the opposite charge of the GUVs membrane during the incubation as already observed in the case of quantum dots.[14] These two experiments suggest that the nanoclusters are adhering to the membranes in agreement with the progressive neutralization of the surface charge observed by Zetametry. In view to precise the exact position of the AuNC nanostructures on the membrane, all the samples were analyzed by SAXS after equilibration of the

resulting structures. A scattering peak at 0.122 $Å^{-1}$ corresponding to the expected membrane thickness of the SUVs (5.1 nm) was observed and was enhanced in presence of oppositely charged NCs (Figure 4d). The highest exaltation of the intensity peak occurs for C_3E_6D AuNC- that strongly interact with DMPC:DMTAP (9:1) SUV+. This increase of the intensity of the scattering signal is attributed to the increasing number of AuNCs adhering electrostatically with the membrane. The observed intensity enhancement is attributed to the high gold atomic number which, by increasing the X-ray scattering contrast, also increasing the signal on the SAXS spectrum. One can also notice a slight increase of the intensity peak with the DMPC SUV (0) which are slightly negatively charged due to the orientation of the phosphatidyl choline headgroup dipole with a mean zeta potential around 10 mV.[37] A final important point is that, although the AuNCs are positioned on the membrane, enhancing the SAXS signal, there is no shift in the peak when the vesicles are in excess. This indicates that NCs do not vary the thickness of the membrane and, due to their ultra-small size, manage to insert themselves between the polar heads of the membrane phospholipids (Figure 4e) without increasing the bilayer thickness in the contrary to others bigger nanoparticles such as quantum dots.[14,15,16] An Avogadro simulation was performed as a rough estimation to evaluate if the NC size permit them to insert at the level of the phosphate

headgroup. A comparison of phosphate headgroup distance with and without NCs is also schematized in Figure S11 showing that the AuNC could be located at the level of phosphate groups.

In conclusion, this study gives an overview of the interaction between ultra-small luminescent gold nanoclusters and lipidic membranes through electrostatic attraction showing that it is possible to induce strong change in membrane structures or not. The synthesis of aqueous bioactivable and PEGylated AuNCs suspensions of various charges were obtained according a two-steps process. The first step consists in the GSH AuNCs preparation in only 2 hours with a dimension of about 2 nm, with a fluorescence excitation peak at 430 nm and an emission peak at 620 nm. Then a ligand exchange step allowed to bind the AuNCs with thiol groups of different ligands in order to functionalize them. Following incubation of the AuNCs with oppositely charged vesicles, either liposomes or EVs, the strong electrostatic attraction resulting in the AuNC adsorption to the membranes was evidenced by complementary techniques such as Zetametry, fluorescence optical microscopy, SAXS and cryo-TEM. In presence of an membrane surface excess, AuNCs do not change the size of the membrane thickness, so they are positioned between the polar headgroups of the membrane phospholipids in the contrary to larger gold nanoparticles.[16] So these ultra-small

and stable gold nanoclusters can serve as biomarkers of lipidic membranes such as human EVs for in-situ biosensing or drug delivery. In presence of an excess of oppositely charged AuNCs, the liposomes strongly adhere the one to each other without disrupting their membrane structure whereas the EVs extracted from human follicular fluid rearrange into an hybrid lamellar phase in presence of oppositely charged nanoclusters. These ultra-small luminescent nanoclusters could serve for the design of new hybrid vectors based on the control of their interaction with specific extracellular vesicles.

FUNDINGS

We are thankful to La Ligue Contre le Cancer for its financial support. We are also thankful to Catania University for its fellowship to R.C. and Rennes1 University for its fellowship to S. D. and its financial support. The authors are grateful to V. Dorcet for the assistance in TEM experiments performed on THEMIS platform and to G. Taupier for the assistance in quantum yields measurements performed on Caphter platform (ScanMAT, UAR 2025 University of Rennes 1-CNRS; CPER-FEDER 2007–2014).

EXPERIMENTAL METHODS

Generals. Human ovarian follicular liquid samples were provided by the Biobank GERMETHEQUE. The PEGylated ligands were prepared and purchased from Agentide (purity (HPLC) 85.624%. All the other chemical compounds and solvents were purchased from Sigma aldrich. The measurements of the mean hydrodynamic diameters were performed at an angle of 173˚ using a Nanosizer ZEN3600 (Malvern Instruments, England) and collected at 25 ˚C, without dilution or filtration. The absorption spectra were performed on a Thermo Scientific™ NanoDrop™ UV-Vis spectrometer. The absolute fluorescence quantum yields were measured usign a C9920–03 Hamamatsu system by exciting the samples at 410 nm.

Au Nanoclusters Synthesis (AuNC). All glassware used for these synthesis were cleaned in a bath of freshly prepared aqua regia (HCl:HNO_3, 3:1 by volume) and rinsed in water 10 times before use. The AuNCs solution obtained could be stored at 4 ˚C for months without significant change in their optical properties. A freshly prepared aqueous solution of glutathione denoted GSH (50 mM, 1,2 mL) were mixed with 16,8 mL of ultrapure water. The solution was heated in oil bath at 120˚C and $HAuCl_4$ (20 mM, 2mL) and was rapidly added. The reaction was stopped after stirring for 3h. An aqueous suspension of orange-emitting GSH AuNCs was formed (2.6 μM). Then a freshly prepared aqueous solution of the desired ligand (20 mM, 1000 eq / Au) (C_3E_6D, K5CNH2

or MUTAB) was incubated overnight in presence of the GSH AuNCs. The obtained AuNCs were purified on centrifugal filter (Amicon-ultra 0.5 device 3kDa, Merk) to remove the ligand excess. Typically, a freshly prepared aqueous solution of C_3E_6D (20 mM, 0.390 mL) was overnight incubated with GSH Au NCs (2.6 μM, 1 mL) suspension in dark at room temperature to obtain the final C_3E_6D AuNCs (denoted AuNC-).

Preparation of Phospholipidic Vesicles (GUV, LUV and SUV).

Large Unilamellar Vesicles (LUVs). Lipidic stock solutions of DOPC (1 mL at 10 mg / mL) and DOTAP (98.5 μL, 10 mg / mL) in dichloromethane were prepared. The appropriated lipidic mixture (total lipid concentration used: 10 mg/mL), either pure DOPC or a molar DOPC:DOTAP (9:1) mixture, was introduced into a 50 mL vial and the organic solvent was evaporated with a rotary evaporator (Büchi Heating Bath) (40 ° C, 100 mbar) to form a lipidic film onto the vial surface during 30 min. Then, an aqueous sucrose solution (1.2 ml, 50 mM) was added, and the suspension was successively placed in a liquid nitrogen bath for 30 s and in a water bath at 40°C for 30 s. The freezing-unfreezing cycle was repeated five times to form the MLV (MultiLamellar Vesicles). This MLV suspension was then extruded 10 times through a 100 nm diameter polycarbonate filter in an extruder (Thermobarrel Extruder Lipex Membrane) under a pressure of

15-10 bar. The mean hydrodynamic diameter of the obtained LUVs was measured to be around 110 ± 20 nm by Dynamic Light Scattering (DLS) (Figure S5a,b).

Small Unilamellar Vesicles (SUVs). a lipid solution is prepared by dissolving 20 mg of DMPC and 1.74 mg of DMTAP in 2 ml of dichloromethane. Using a rotary evaporator (Buchi Heating Bath), the dichloromethane is evaporated (40 ˚ C, 100 mbar) and an aqueous sucrose solution (2 ml, 50 mM) is added to hydrate the as-formed lipidic film. The solution obtained is sonicated using a titanium ultrasonic probe (Misonix Incorporated) placed at maximum power for 30 minutes. After centrifugation at 7500 g for 10 minutes to eliminate the possible titanium traces, the supernatant is then removed and the SUV solution is ready for use. The SUVs average size estimated by Dynamic Light Scattering was 46± 16 nm (Figure S5c,d).

Giant unilamellar vesicles (GUVs).[36] A lipid solution was prepared dissolving DOPC or DOPC:DOTAP (95:5) molar lipidic mixture lipids in chloroform (10 mg / ml). 20 µL of this solution and 1.8 mL of paraffin oil are mixed and heated at 80 ˚ C for 30 min in a flask without cap. Then, the suspension is placed in a desiccator for 20 min in order to evaporate the chloroform and to obtain the final lipid organic solution. To prepare the GUV, 50 µL of sucrose (500 mM) are added to 400 µL of lipid solution vortexed for 40 s to form a water-in-oil (w/o) emulsion. Then,

this emulsion is gently added on the top of a sucrose solution of high viscosity (200 µL, 500 mM in a second Eppendorf) without mixing. After waiting 10 minutes, the solution is centrifuged for 15 minutes at 18890 g The bottom was transferred into another Eppendorf, redispersed in 300 µl of glucose (500 mM) and centrifuged again at 18890 g for 5 minutes. After centrifugation, the bottom solution is taken up and the GUVs are ready to be stored in the refrigerator.

Small-Angle X-ray Scattering (SAXS). X-ray patterns were collected with a Mar345 Image-Plate detector (Maresearch, Norderstedt, Germany) mounted on a rotating anode X-ray generator FR591 (Bruker, Courtaboeuf, France) operated at 50 kV and 50 mA. The sample to detector distance (422 mm) has been calibrated by using silver behenate. The X-ray patterns were therefore recorded for a range of reciprocal spacing $q = 4\pi \sin\theta/\lambda$ from is 0.04-1.2 $Å^{-1}$ where θ is the diffraction angle. The experiments performed with the present set-up provide accurate measurements of distances between 150 Å and 5.2 Å. The acquisition time was 1 hour. Samples were loaded in thin Lindman glass capillaries (diameter 1 ± 0.1 mm and thickness 10 µm; GLAS, Muller, Berlin, Germany) sealed with paraffin. The lipid-NCs hybrid complexes were prepared by mixture of a micromolar concentration NCs solution (10 µL, 1.70 µM NCs concentration) and millimolar concentration SUV suspension (10 µL, 16 mM total phospholipid concentration) in the

glass capillaries. All samples exhibited powder diffraction rings, and the scattering intensities as a function of the radial wave vector were determined by circular integration.

Zeta Potential measurements. The zeta potential measurements were performed using the Zetasizer ZEN3600 (Malvern Instruments, England) equipped with a He-Ne laser source (λ=633 nm). Millimolar concentration solutions of vesicles were loaded into disposable folded capillary cells Zeta Cell (DTS 1060) and data were collected at 25 ˚C. A 3 mM vesicle solution was diluted 3 times with 25 mM NaCl to give a 1mM vesicle solution. Its zeta potential was measured and then a few μL of NCs (8.7 μM diluted 3 times with 25 mM of NaCl) was added little by little by making a titration and measuring the zeta potential after each addition. The vesicles zeta potential was extracted from the inelastic frequency shift of the laser signal scattered by moving charged colloid under an electric field (applied cell voltage was 15 V).

Spectrofluorimetry. Photoluminescence measurements were performed on a Jasco FP-8300 spectrofluorometer. The measurements were performed at room temperature on liquid samples. The wavelength resolution of both the excitation and the emission slits was set to 5 nm, the response times was 0.5 s, the detector sensitivity was set to medium and the scan speed was 500 nm/min.

Luminescence Lifetime measurements. Luminescence measurements were performed by pumping with the 325 nm line of an HeCd laser. The pump power was 0.6 mW over a circular area with a 1 mm diameter and the laser beam was chopped through an acousto-optic modulator at a frequency of 55 Hz. The luminescence signal was analyzed by a single grating monochromator and detected by a photomultiplier tube. Luminescence lifetime measurements were performed by detecting the luminescence signal at 600 nm after pumping to steady state, switching off the laser beam and analyzing it with a photon counting multichannel scaler having the signal from the modulator as a trigger.

Light Optical Microscopy. The fluorescence optical microscopy observations were performed either under direct bright light and epifluorescence on an inverted microscope IX71 (Olympus, Japan) equipped with both a 20 x, 0.45 (NA) objectives (Olympus, Japan). NCs solutions were excited at 365 nm by a high vacuum mercury lamp (200 W). Images were acquired by a Photometrics CoolSNAP HQ2 camera equipped with a soft imaging system (Olympus, Japan).

Transmission Electron Microscopy (TEM). Transmission Electron Microscopy analysis were carried out with with JEOL 2100 transmission electron microscope operated at 200 KV supplied with UltraScan 1000XP CCD Camera. For the sample preparation, 300 mesh carbon coated nickel

grids were placed for 1 min on top of a 40 µL sample droplet and dried up with paper. Particle sizes and interparticle distances were determined from TEM micrographs using Fiji Software.

Cryo-Transmission Electron Microscopy (Cryo-TEM). Vitrification of vesicles was performed using an automatic plunge freezer (EM GP, Leica) under controlled humidity and temperature (Dubochet and McDowall, 1981). The samples were deposited to glow-discharged electron microscope grids followed by blotting and vitrification by rapid freezing into liquid ethane. Grids were transferred to a single-axis cryo-holder (model 626, Gatan) and were observed using a 200 kV electron microscope (Tecnai G^2 T20 Sphera, FEI) equipped with a 4k × 4k CCD camera (XF416, TVIPS). Micrographs were acquired under low electron doses using the camera in binning mode 1 and at a nominal magnifications of 25,000x.

SUPPORTING INFORMATION

Figure S1: AuNCs fluorescence spectra, fluorescence lifetime and size distribution histogram ; Figure S2: Image of lyophilized AuNCs ; Figure S3 : Chemical structures of AuNCs ligands ; Figure S4 : Excitation and emission Intensity spectra of AuNCs before and after ligand exchange and purification, DLS and fluorescence spectrum showing the stability of AuNCs after 4 months ;

Figure S5: FT-IR spectra of the purified C_3E_6D-AuNC and GSH-AuNC as well as C_3E_6D and GSH alone. Figure S6 : DLS measurements of LUVs and SUVs ; Figure S7 : zeta potential titration of LUV+ with K_5CNH_2 and C_5PEG_4 AuNCs ; Figure S8 : SAXS spectra of SUV+ and DMPC SUV interacting with Au NC+ or Au NC-; Figure S9: SAXS spectra of EVs interacting with Au NC+ or Au NC- ; Figure S10 : SAXS of MUTAB alone or in presence of EVs; Figure S11 : Avogadro simulation of AuNCs interacting with membrane phospholipids.

Notes

The authors declare no competing financial interests.

REFERENCES

(1) Wang, J.; Ye, J.; Jiang, H.; Gao, S.; Ge, W.; Chen, Y.; Liu, C.; Amatore, C.; Wang, X. Simultaneous and Multisite Tumor Rapid-Target Bioimaging through in Vivo Biosynthesis of Fluorescent Gold Nanoclusters. *RSC Adv.* **2014**, *4* (71), 37790–37795.

(2) Nonappa. Luminescent Gold Nanoclusters for Bioimaging Applications. *Beilstein J. Nanotechnol.* **2020**, *11* (1), 533–546.

(3) Cui, H.; Shao, Z.-S.; Song, Z.; Wang, Y.-B.; Wang, H.-S. Development of Gold Nanoclusters: From Preparation to Applications in the Field of Biomedicine. *J. Mater. Chem. C* **2020**, *8* (41), 14312–14333.

(4) Zhang, X.-D.; Luo, Z.; Chen, J.; Song, S.; Yuan, X.; Shen, X.; Wang, H.; Sun, Y.; Gao, K.; Zhang, L.; Fan, S.; Leong, D. T.; Guo, M.; Xie, J. Ultrasmall Glutathione-Protected Gold Nanoclusters as Next Generation Radiotherapy Sensitizers with High Tumor Uptake and High

Renal Clearance. *Sci. Rep.* **2015**, *5* (8669), 1-6.

(5) Loynachan, C. N.; Soleimany, A. P.; Dudani, J. S.; Lin, Y.; Najer, A.; Bekdemir, A.; Chen, Q.; Bhatia, S. N.; Stevens, M. M. Renal Clearable Catalytic Gold Nanoclusters for in Vivo Disease Monitoring. *Nat. Nanotechnol.* **2019**, *14* (9), 883–890.

(6) Zhang, X.-D.; Wu, D.; Shen, X.; Liu, P.-X.; Fan, F.-Y.; Fan, S.-J. In Vivo Renal Clearance, Biodistribution, Toxicity of Gold Nanoclusters. *Biomaterials* **2012**, *33* (18), 4628–4638.

(7) Liang, G.; Jin, X.; Zhang, S.; Xing, D. RGD Peptide-Modified Fluorescent Gold Nanoclusters as Highly Efficient Tumor-Targeted Radiotherapy Sensitizers. *Biomaterials* **2017**, *144*, 95–104.

(8) Tao, Y.; Li, M.; Kim, B.; Auguste, D. T. Incorporating Gold Nanoclusters and Target-Directed Liposomes as a Synergistic Amplified Colorimetric Sensor for HER2-Positive Breast Cancer Cell Detection. *Theranostics* **2017**, *7* (4), 899–911.

(9) Porret, E.; Sancey, L.; Martín-Serrano, A.; Montañez, M. I.; Seeman, R.; Yahia-Ammar, A.; Okuno, H.; Gomez, F.; Ariza, A.; Hildebrandt, N.; Fleury, J.-B.; Coll, J.-L.; Le Guével, X. Hydrophobicity of Gold Nanoclusters Influences Their Interactions with Biological Barriers. *Chem. Mater.* **2017**, *29* (17), 7497–7506.

(10) Chatterjee, A.; Purkayastha, P. The Impact of Lipid Head-Groups in GUVs on Electron Transfer by Surface-Adsorbed Fluorescent Gold Nanoclusters. *Mater. Adv.* **2021**, *2* (4), 1343–1350.

(11) Porret, E.; Fleury, J.-B.; Sancey, L.; Pezet, M.; Coll, J.-L.; Le Guével, X. Augmented Interaction of Multivalent Arginine Coated Gold Nanoclusters with Lipid Membranes and Cells. *RSC Adv.* **2020**, *10* (11), 6436–6443.

(12) Porret, E.; Le Guével, X.; Coll, J.-L. Gold Nanoclusters for Biomedical Applications: Toward *in Vivo* Studies. *J. Mater. Chem. B* **2020**, *8* (11), 2216–2232.

(13) Kauscher, U.; Penders, J.; Nagelkerke, A.; Holme, M. N.; Nele, V.; Massi, L.; Gopal, S.; Whittaker, T. E.; Stevens, M. M. Gold Nanocluster Extracellular Vesicle Supraparticles: Self-Assembled Nanostructures for Three-Dimensional Uptake Visualization. **2020**, *Langmuir*, *36* (14), 3912-3923.

(14) Dif, A.; Henry, E.; Artzner, F.; Baudy-Floc'h, M.; Schmutz, M.; Dahan, M.; Marchi-Artzner, V. Interaction between Water-Soluble Peptidic CdSe/ZnS Nanocrystals and Membranes: Formation of Hybrid Vesicles and Condensed Lamellar Phases. *J. Am. Chem. Soc.* **2008**, *130* (26), 8289–8296.

(15) Bizien, T.; Ameline, J.-C.; Yager, K. G.; Marchi, V.; Artzner, F. Self-Organization of Quantum Rods Induced by Lipid Membrane Corrugations. *Langmuir* **2015**, *31* (44), 12148–12154.

(16) Contini, C.; Hindley, J. W.; Macdonald, T. J.; Barritt, J. D.; Ces, O.; Quirke, N. Size Dependency of Gold Nanoparticles Interacting with Model Membranes. *Commun. Chem.* **2020**, *3* (130), 1-12.

(17) Hung, W.-T.; Navakanitworakul, R.; Khan, T.; Zhang, P.; Davis, J. S.; McGinnis, L. K.; Christenson, L. K. Stage-Specific Follicular Extracellular Vesicle Uptake and Regulation of Bovine Granulosa Cell Proliferation†. *Bio. Reprod.* **2017**, *97* (4), 644–655.

(18) Yefimova, M. G.; Béré, E.; Cantereau-Becq, A.; Meunier-Balandre, A.-C.; Merceron, B.; Burel, A.; Merienne, K.; Ravel, C.; Becq, F.; Bourmeyster, N. Myelinosome Organelles in the Retina of R6/1 Huntington Disease (HD) Mice: Ubiquitous Distribution and Possible Role in Disease Spreading. *Int. J. Mol. Sci.* **2021**, *22* (23), 12771-12794.

(19) Neyroud, A.-S.; Chiechio, R.; Yefimova, M.; Lo Faro, M. J.; Dejucq-Rainsford, N.; Jaillard, S.; Even-Hernandez, P.; Marchi, V.; Ravel, C. Extra-Cellular Vesicles of the Male Genital Tract: New Actors in Male Fertility? *Basic Clin. Androl.* **2021**, *31* (1), 25-34.

(20) Bourmeyster, N. Myelinosome-Driven Secretion: Non-Catabolic Management of Misfolded Proteins - Lessons from the Sertoli Cells. *J Rare Dis Res Treat* **2017**, *2* (2), 24–27.

(21) Yefimova, M. G.; Béré, E.; Cantereau-Becq, A.; Harnois, T.; Meunier, A.-C.; Messaddeq, N.; Becq, F.; Trottier, Y.; Bourmeyster, N. Myelinosomes Act as Natural Secretory Organelles in Sertoli Cells to Prevent Accumulation of Aggregate-Prone Mutant Huntingtin and CFTR. *Hum. Mol. Genet.* **2016**, *25* (19), 4170–4185.

(22) Beach, A.; Zhang, H.-G.; Ratajczak, M. Z.; Kakar, S. S. Exosomes: An Overview of Biogenesis, Composition and Role in Ovarian Cancer. *J. Ovar. Res.* **2014**, *7* (14), 1-10

(23) Bai, Y.; Lu, Y.; Wang, K.; Cheng, Z.; Qu, Y.; Qiu, S.; Zhou, L.; Wu, Z.; Liu, H.; Zhao, J.; Mao, H. Rapid Isolation and Multiplexed Detection of Exosome Tumor Markers Via Queued Beads Combined with Quantum Dots in a Microarray. *Nano-Micro Letters* **2019**, *11* (59), 1-11.

(24) Cheng, J.; Nonaka, T.; Wong, D. Salivary Exosomes as Nanocarriers for Cancer Biomarker Delivery. *Materials* **2019**, *12* (654), 1-18.

(25) Luo, Z.; Yuan, X.; Yu, Y.; Zhang, Q.; Leong, D. T.; Lee, J. Y.; Xie, J. From Aggregation-Induced Emission of Au(I)–Thiolate Complexes to Ultrabright Au(0)@Au(I)–Thiolate Core–Shell Nanoclusters. *J. Am. Chem. Soc.* **2012**, *134* (40), 16662–16670.

(26) Gurunatha, K. L.; Fournier, A. C.; Urvoas, A.; Valerio-Lepiniec, M.; Marchi, V.; Minard,

P.; Dujardin, E. Nanoparticles Self-Assembly Driven by High Affinity Repeat Protein Pairing. *ACS Nano* **2016**, *10* (3), 3176–3185.

(27) Piñeiro, Y.; Rivas, J.; López-Quintela, M. A. The Emergence of Quantum Confinement in Atomic Quantum Clusters. In *Colloids Foundations of Nanoscience*; edited by D. Berti and G. Palazzo, Elsevier, 2014; 81–105.

(28) Huang, Y.; Fuksman, L.; Zheng, J. Luminescence Mechanisms of Ultrasmall Gold Nanoparticles. *Dalton Trans.* **2018**, *47* (18), 6267–6273.

(29) Oh, E.; Huston, A. L.; Shabaev, A.; Efros, A.; Currie, M.; Susumu, K.; Bussmann, K.; Goswami, R.; Fatemi, F. K.; Medintz, I. L. Energy Transfer Sensitization of Luminescent Gold Nanoclusters: More than Just the Classical Förster Mechanism. *Sci. Rep.* **2016**, *6* (35538), 1-17

(30) Hamon, C.; Postic, M.; Mazari, E.; Bizien, T.; Dupuis, C.; Even-Hernandez, P.; Jimenez, A.; Courbin, L.; Gosse, C.; Artzner, F.; Marchi-Artzner, V. Three-Dimensional Self-Assembling of Gold Nanorods with Controlled Macroscopic Shape and Local Smectic B Order. *ACS Nano* **2012**, *6* (5), 4137–4146.

(31) Fernandez, M.; Urvoas, A.; Even-Hernandez, P.; Burel, A.; Mériadec, C.; Artzner, F.; Bouceba, T.; Minard, P.; Dujardin, E.; Marchi, V. Hybrid Gold Nanoparticle–Quantum Dot Self-Assembled Nanostructures Driven by Complementary Artificial Proteins. *Nanoscale* **2020**, *12* (7), 4612–4621.

(32) Stamplecoskie, K. G.; Chen, Y.-S.; Kamat, P. V. Excited-State Behavior of Luminescent Glutathione-Protected Gold Clusters. *J. Phys. Chem. C* **2014**, *118* (2), 1370–1376.

(33) Oh, E.; Fatemi, F. K.; Currie, M.; Delehanty, J. B.; Pons, T.; Fragola, A.; Lévêque-Fort, S.; Goswami, R.; Susumu, K.; Huston, A. L.; Medintz, I. L. PEGylated Luminescent Gold Nanoclusters: Synthesis, Characterization, Bioconjugation, and Application to One- and Two-Photon Cellular Imaging. *Particle & Particle Syst. Charac.* **2013**, *30* (5), 453–466.

(34) Pyo, K.; Thanthirige, V. D.; Kwak, K.; Pandurangan, P.; Ramakrishna, G.; Lee, D. Ultrabright Luminescence from Gold Nanoclusters: Rigidifying the Au(I)–Thiolate Shell. *J. Am. Chem. Soc.* **2015**, *137* (25), 8244–8250.

(35) Wu, Z.; Jin, R. On the Ligand's Role in the Fluorescence of Gold Nanoclusters. *Nano Letters* **2010**, *10* (7), 2568–2573.

(36) Matsushita-Ishiodori, Y.; Hanczyc, M. M.; Wang, A.; Szostak, J. W.; Yomo, T. Using Imaging Flow Cytometry to Quantify and Optimize Giant Vesicle Production by Water-in-Oil Emulsion Transfer Methods. *Langmuir* **2019**, *35* (6), 2375–2382.

(37) Disalvo, E. A.; Bouchet, A. M. Electrophoretic Mobility and Zeta Potential of Liposomes Due to Arginine and Polyarginine Adsorption. *Coll. Surf. A: Phys. Eng. Asp.* **2014**, *440*, 170–174.